Characterisation of hypersaline zones in salt marshes

Chengji Shen[1], Yu Fan[1], Chunhui Lu[2], Jun Kong[1], Yue Liu[3], Ling Li[4], Chenming Zhang[3,#]

[1]College of Harbour, Coastal and Offshore Engineering, Hohai University, Nanjing, China.

[2]Yangtze Institute for Conservation and Development, Hohai University, Nanjing, China.

[3]School of Civil Engineering, The University of Queensland, Brisbane, Australia.

[4]College of Engineering, Westlake University, Hangzhou, China.

[#]Corresponding author: Chenming Zhang (chenming.zhang@uq.edu.cn)

Submitted to ***Geophysical Research Letters*** on **14/02/2022**

Abstract

Salt pans are commonly found in coastal marshes and play a vital role in the marsh plants zonation. However, the correlation between these hypersaline zones and the marsh hydrological conditions have barely been characterized. This study numerically investigates the effects of evaporation rate, tidal amplitude, and marsh platform slope on salt pan formation, and found that salt pans can hardly grow in the intertidal zone due to regular tidal flushing, while tend to form in the lower supratidal zone, where evaporation is sustained. The accumulated salts create an upward salinity gradient that trigger downward unstable flow. The decreases of potential evaporation rate, tidal amplitude and/or marsh platform slope strengthen the hydraulic connection between the marsh surface and the underlying watertable, the key to sustaining evaporation, and therefore result in thickener and wider salt pans. These findings offer a deeper insight into the marsh ecohydrology and guidance for their degradation prevention.

Keywords: Salt marshes; salt pans; salinity distribution; evaporation; plant zonation; coastal wetlands.

Plain Language Summary

Salt marshes at the land-ocean interface are ecologically valuable wetlands. The various eco-functions of salt marshes are closely linked to the marsh plants, which usually exhibit striking zonation patterns across elevational gradients. Salinity distributions are regarded as an important physical stressor determining plant zonation in salt marshes. In particular, under certain conditions, hypersaline salt pans will form in the supratidal zones of salt marshes, completely inhibiting plant growth due to the extremely high salinity. Despite the ecological significance, the characteristics of salt pans remain poorly understood, and this study numerically explores this topic. The results show that the location and width of salt pans are both quite sensitive to potential evaporation rate, tidal amplitude and the slope of marsh surface. These research findings may provide guidance for preventing salt marshes from degradation.

39

Highlights:

- salt pans cannot grow in intertidal zone due to tidal flushing, while tend to form in lower supratidal zone, where evaporation is sustained
- Downward unstable fingering helps dissipate the salt accumulation by evaporation, therefore stabilize the surface salinity
- The decreases of potential evaporation rate, tidal amplitude and/or marsh platform slope result in thickener and wider salt pans

1. Introduction

Salt marshes at the ocean-land interface are one of the most productive ecosystems worldwide, since they provide numerous eco-functions, e.g., maintaining coastal biodiversity (Adam, 1990) and protecting inland area from the threat of sea level rise (Kirwan & Megonigal, 2013). These eco-functions are closely linked to marsh plants, which have been found to exhibit striking zonation patterns across elevational gradients in many salt marshes (Chapman, 1974). Various studies were carried out to understand the underlying mechanisms and major drivers of plant zonation. Generally, it is believed that physical stress, rather than biotic interactions, greatly affects the distribution pattern of marsh plants (Bertness & Pennings, 2000; Emery et al., 2001). For example, He et al. (2012) found that, due to the harsh physical conditions of high estuarine marshes in the Yellow River Delta, the invasion of *Spartina* is limited to low estuarine marshes only.

Salinity is an important physical stressor controlling plant zonation, because different species vary greatly in their salt tolerance levels. Pennings et al. (2005) concluded that, for low-latitude salt marshes, salinity may determine the distributional limit of *Spartina*. The importance of salinity in affecting zonation was also highlighted by Moffett et al. (2010a), who rated salinity changes as the most effective metrics for distinguishing species habitats and halophytes zones in the marsh site they investigated. The hypothesized the link between salinity variations and zonation has driven various studies in the form of field measurements, laboratory experiments and

numerical modeling. Laboratory experiments under controllable conditions have demonstrated that excess salinity is stressful to angiosperms (Noe, 2002; Noe & Zedler, 2000; Pennings & Moore, 2001). While field and numerical studies showed that soil surface salinity in salt marshes increases with marsh surface elevation towards landward and reaches the maxima just above the mean high sea level (MHSL), beyond which the soil surface salinity starts decreasing (Adam, 1990; Mahall & Park, 1976; Wang et al., 2007). Such a consistent cross-shore salt distribution pattern is due to that longer evaporation periods at higher elevations lead to salts rather concentrated in surface soil, while the barely flooded areas above the MSHL receives much less salt load. These results can partially explain the zonation by linking topographic elevation and the distribution of halophytes, of which the responses to salinity are quite species-dependent.

In some salt marshes, however, instead of decreasing, the surface soil salinity beyond MSHL may continue rising to a high level and result in salt precipitate on the marsh surface. Consequently, a hypersaline and non-vegetative zone called salt pan (alternatively known as salt barren or salt flat, Figures 1a-1b) will form. The non-vegetative feature makes salt pans rather discernible from satellite or aerial images. Due to the inhibitory effect on plant growth, salt pans have received wide attention from many studies, with an attempt to understand the formation mechanisms of these plant-suppressive areas. Based on field data of salt pans in a *Juncus* marsh of northwestern Florida, Hsieh (2004) developed a theory of salt pan formation, where salt pans tend to be found in tide-dominated salt marshes and the mean high water (MHW) level dictates the position of a salt pan. Hsieh (2004) called for mechanism-based modeling studies to test the theory and unravel important insights into the formation of salt pans. Wang et al. (2007) modified a salt and water balance model to simulate the effects of soil, tides, topography and climate on the salt dynamics of the Atlantic and Gulf coastal marshes. Their simulation results indicate that the mean higher high water (MHHW) level determines the position of the salinity plateau, while the tidal irregularity affects the width of the salinity plateau. More importantly, Wang

et al. (2007) found that salt pans may form once the maximum salinity reaches a threshold under the influences of hydraulic conductivity, temperature, evaporation and tidal salinity. Nonetheless, the underlying mechanism of salt pan formation remains unclear, since their model only simulates salinity variations without considering salt accumulation and precipitation in marsh soils and on marsh surfaces. More recently, Shen et al. (2018) numerically investigated the salt dynamics in coastal marshes with a focus on salt pans. Their simulations highlighted the importance of the hydraulic connection between the watertable and marsh surface, which sustains evaporation and so supports salt pan formation in the supratidal zone. In situations of high potential evaporation rates or low marsh soil permeability, the hydraulic connection cannot be maintained and evaporation will be disrupted, thereby impeding the formation of salt pans. These findings provide an important insight into the mechanism of salt pan development.

Although previous studies have revealed the complexity of salt pan formation, there lacks a systemic investigation to characterize these hypersaline zones of great ecological importance. A more enhanced understanding of salt pans and possibly their link to plant zonation in salt marshes is urgently needed. This study numerically characterized salt pans in tidal marshes by simulating and analyzing salinity distribution patterns in a 2-D creek-normal section representative of natural salt marshes. Three key controlling variables were examined, including slope of marsh platform, potential evaporation rate and tidal amplitude.

2. Methods

This study conducted the numerical simulations using SUTRASET (Shen et al., 2018; Zhang et al., 2014). SUTRASET was modified based on the variable-saturation, variable-density groundwater model SUTRA (Voss & Provost, 2008), by incorporating an evaporation module to simulate the salt accumulation/precipitation process in porous medium. More details of the SUTRASET model are provided by Zhang et al. (2014) and Shen et al. (2018).

2.1. Model Setup

This study considered a 2-D soil section perpendicular to a creek in a tide-dominated salt marsh (Figure 1c). By neglecting inland freshwater input, the inland boundary AB was set to be no-flow. The marsh bottom AF and the hydraulic divide EF were also set as no-flow boundaries. The boundary conditions of the marsh platform BC and tidal creek CDE were determined according to the tidal level and local porewater saturation conditions: (1) hydrostatic pressure boundary was applied to the section underneath the tides; (2) a seepage with an atmospheric pressure was prescribed for the saturated section above the tidal level during falling tide, following the approach of Wilson and Gardner (2006); and (3) evaporation was applied to the exposed unsaturated section. Evaporation of seawater is neglected in the model as it affects little the seawater salinity.

For simplicity, this study adopted a semi-diurnal tidal signal that is given as:

$$h_{\text{tide}} = h_{\text{msl}} + A\sin(\omega t) \quad (1)$$

where h_{tide} [L] is the tidal level that varies with time t [T], h_{msl} [L] is the mean sea level (MSL) and was set to 4.5 m in all simulations, A [L] is the tidal amplitude, ω [-] is the angular frequency of tides and $\omega=2\pi/T$, with T [T] being the tidal period and set to 12 hr. The initial hydraulic heads in the entire model domain were set as hydrostatic based on the MSL. Also, an initial porewater salinity of 35 ppt (parts per thousand) was applied to whole domain.

2.2. Simulation Cases and Parameter Ranges

Hsieh (2004) identified that the physical factors involving surface topography, tide regime and local climate are critical to the formation of salt pans in salt marshes. Therefore, this study examined three major controlling variables: tidal amplitude (A), potential evaporation rate (EVP), and slope of marsh platform (S_p). Tidal amplitudes were varied between 0.7-1.6 m, with an interval of 0.3 m. The potential evaporation rates were set to 2 mm day^{-1}, 4 mm day^{-1}, 6 mm day^{-1} and 8 mm day^{-1}, respectively. Three marsh platforms slopes were chosen, being 0.01, 0.02 and 0.03. All these values

are listed in Table S1, leading to a total of 48 simulation cases. The marsh top soil was assumed to be homogeneous and sandy loam, a commonly found soil type in coastal marshes due to tides that brought in varying ranges of sediments and vegetations that accumulate them around the root zones. With stronger water retaining capacity than sands which are critical for evapoconcentration, and higher permeability than clays which are important to replenish evaporated porewater, sandy loam has a unique characteristic that promotes the formations of salt pans.

The same mesh discretization scheme with 36491 nodes and 36000 elements were adopted in all simulations to ensure that the grid Péclet number (P_e) could satisfy the stability criterion ($P_e \leq 4$) for avoiding numerical oscillations (Hughes & Sanford, 2004). Meanwhile, a 60-s time step size was used. Tests on the dependence of results on mesh and time step size were conducted to ensure such a model setup generates numerically converged results with relatively high computational efficiency. The model was allowed to simulate salt dynamics driving by tide and evaporation over 5 years. Although the simulations did not reach a quasi-steady state completely, where the total amount of salts in the soil does not change over time, the surface salinity and thickness of precipitated salt changed rather slowly if the simulation continued.

3. Results and Discussions

Figure 2 shows the time-dependent variations of evaporation rate, saturation, concentration and salt thickness on the soil surface, and salinity distributions in the marsh soil. The liquid water saturation over time does not change over time, indicating the flow condition reaches a steady station condition in less than a month. On the marsh platform starting from the creek bank, the surface saturation increases with elevation and reaches a maximum at the middle of the intertidal zone. Such rising saturation pattern was formed by porewater circulation, where saltwater infiltrates the unsaturated marsh soil from the marsh platform, and discharge from the creek bank. The porewater circulation weakens as the distance to the creek increases, resulting in higher saturation. Further landward to the saturation maxima, the surface saturation declines with elevation due to less inundation period and hence limited

recharge. Within the intertidal zone, salinity remains near 35 ppt and salt precipitation is absent, as the tide can flush the salts accumulated by intermittent evaporation. Due to abundant moisture and no salt stress, the evaporation rate in the intertidal zone is maintained close to the potential rate. Despite never being inundated, the supratidal zone between 60 m < x <130 m maintains a surface saturation above 0.5, as the local water table is rather close to the surface. The high surface moisture availability leads to persistent evaporation, which takes water away with salt left behind, resulting in the formation of a salt pan on the surface. In turn, salt accumulation reduces the evaporation rate evidently in the supratidal zone. Such an inhibitory effect of salt accumulation on evaporation rate has been previously reported by America et al. (2020). At the very early stage (e.g., 0.07 year, Figure 2a), salinity near the marsh surface gradually increases but does not reach a high level. As evaporation continues, salts underneath the marsh surface become more concentrated (e.g., 1.03 years, Figure 2b), creating significant density gradients vertically. Consequently, the salt plume sinks through the unsaturated zone (above the watertable represented by the white dashed line), penetrating and forming salt fingering below the watertable. These salt fingers merge as they move towards the marsh bottom, finally forming a sand-clock shaped plume that spreads laterally (Figures 2c-2f). Further inland to the salt pan (where x < 60m), surface saturation reduced to nearly zero, due to the disruption of the hydraulic connection between the surface and water table disrupts. As a consequence, evaporation and excess salts are absent in that region.

Salt fingering in coastal marshes have been reported by several studies. In their investigations on the drivers of groundwater flow at a marsh-back barrier island transect, Ledous et al. (2013) has pointed out the potential occurrence of salt fingering induced by high salinity, stating that "*high temperatures can cause a high amount of evaporation across the marsh and salinities in saltpans can reach 60 ppt during parts of the year, potentially inducing salt fingering*". Shen et al. (2015) numerically discovered that, when the salinity of surface water is higher than that of subsurface water, in certain situations, unstable fingering would occur in salt marshes, greatly

212 modifying the porewater regime, particularly for the marsh interior near the inland
213 boundary. In addition, the study of Xin et al. (2017) regarding the impact of
214 evaporation, tidal fluctuations and rainfall on marsh soil conditions also reported the
215 formation of salt fingering as salts become very concentrated on the marsh surface.
216 However, both Shen et al. (2015) and Xin et al. (2017) did not consider the process of
217 evaporation-induced salt precipitation on the marsh surface. This study demonstrates
218 how salt accumulation may result in salt fingering under the effect of evaporation,
219 thereby advocating the statement of Ledous et al. (2013).

220 Figures 3(a1)-3(d3) compare the distributions of marsh surface salinity estimated by
221 different cases. Clearly, surface salinity variations in all these cases exhibit a similar
222 spatial pattern: a slight increase with the surface elevation in the intertidal zone, and a
223 sharp increase beyond the MHSL (vertical gray dashed line) to reach the plateau
224 before falling back to 35 ppt in the supratidal zone. Generally, with the tidal amplitude
225 and marsh platform slope unchanged, a higher potential evaporation rate leads to
226 higher surface salinity (i.e., Figure 3(a1)), since more freshwater is evaporated from
227 the salty porewater with salt left behind. Meanwhile, the rise of overall surface
228 salinity is more prominent when the potential evaporation rate increases from a
229 relatively small (e.g., 2 mm day^{-1}) to a moderate value (e.g., 4 mm day^{-1}). Moreover,
230 under the same tidal amplitude and marsh platform slope, the salinity plateau is
231 narrower when the potential evaporation rate is higher, with the seaward end
232 remaining at the MHSL while the landward end shifting further seaward. This is
233 because that, as the topographic elevation increases landward (Figure 1c), the distance
234 between marsh surface and watertable generally increases accordingly. In this regard,
235 at higher elevations, the hydraulic connection between the evaporating surface and
236 underlying watertable, critical for sustaining evaporation, as pointed out by Shen et al.
237 (2018), is disrupted more easily by a high potential evaporation rate. Consequently,
238 evaporation ceases at more elevated areas when the potential evaporation rate is high.

239 The comparison in Figures 3(a1)-3(d3) further demonstrates that, the salinity plateau
240 becomes narrower when the marsh surface is steeper (e.g., Figures 3 (a1), (a2) and

(a3)). Such a trend is also linked to the above-mentioned hydraulic connection, which dictates the location of the right end of the salinity plateau. Therefore, the steeper the marsh surface is, the closer the location of such a critical distance is to the boundary between the supratidal zone and the intertidal zone.

Another notable trend from Figure 3 is that, under the same marsh platform slope and potential evaporation rate, the increase of tidal amplitude narrows the salinity plateau. This trend can be manifested in the comparison between Figures 3(a1), 3(b1), 3(c1) and 3(d1). When tidal amplitude increases, the boundary between supratidal and intertidal zones shifts landward, but the tidal signal attenuates more quickly as it transports landward. As a result, the overall distance between marsh surface and watertable in the supratidal zone becomes greater, resulting in weaker hydraulic connections that maintains evaporation and subsequently narrower salt pans. Moreover, when the tidal forcing is stronger, the location of the salinity plateau shift landward (e.g., Figure 3(a1) vs Figure 3(b1)). According to Hsieh (2004), in event of sea level rise, the upper boundary of salt pan tends to invade into the old high marsh while the corresponding lower boundary may invade into the old salt pan, which are consistent with our results, as the effect of increasing tidal amplitude (with MSL unchanged) on modifying the width and location of salinity plateau is equivalent to that of sea level rise (with tidal amplitude unchanged).

Apart from surface salinity distributions, the present study further compared the maximum surface salinity in different cases. Figures 3(e1)-3(e3) show that, for given potential evaporation rate and marsh surface slope, the highest salinity decreases monotonously with the increase of tidal amplitude. Moreover, the maximum salinity increases by a relatively great extent as the potential evaporation rate rises from 2 mm day^{-1} to 4 mm day^{-1}. However, the increase of maximum salinity is much less sensitive when the potential evaporation rate further increases (e.g., Figure 3(e1)). Among all the cases, the maximum salinity is the greatest when tidal amplitude is 0.7 m, potential evaporation rate is 8 mm day^{-1}, marsh platform slope is 0.01 (Figure 3(e1)). This situation possibly foster an optimal hydraulic connection between the

marsh surface and the watertable for sustaining evaporation.

Based on the exponential ratio between solid and solute salts (used in the SUTRASET model) and simulated surface salinities, this study calculated and plotted the distribution of precipitated salt thickness along the marsh surface (Figures 4(a1)-4(d3)). The section where the solid salt thickness is nonzero represents the salt pan. Apparently, the landward and seaward boundaries of salt pans formed in all the cases are within the corresponding salinity plateaus shown in Figure 3. This is consistent with the findings of Hsieh (2004) that salt pans are confined to the salinity plateau. It is clear from Figures 4(a1)-4(d3) that, in all the simulated cases, the thickness of precipitated salt in the supratidal zone increases first and then decreases towards the landward boundary. Another common feature is that, as the potential evaporation rate increases (tidal amplitude and slope of marsh platform remain the same), the salt precipitating on the marsh surface will be thicker (e.g., Figure 4(a1)). The comparison between Figures 4(a1)-4(d3) indicates that, when a salt pan form in the supratidal zone of a salt marsh, it tends to be thicker when the potential evaporation rate is high (e.g., $EVP = 8$ mm day^{-1}), the tidal amplitude is small (e.g., $A = 0.7$ m), and the marsh surface is mildly sloping (e.g., $S_p = 0.01$).

Using the results of precipitated salt thickness, we calculated the salt pan widths in different cases, based on the thickness criterion of 1×10^{-4} m. Although the use of another criterion may somewhat change the calculated salt pan width, the trend would keep the same. It is evident from Figures 4(e1)-4(e3) that, when tidal amplitude increases while the other two controlling variables stay the same, the variation of salt pan width almost exhibits a linear decreasing trend. More importantly, in accordance with Figure 3, despite the larger surface salinity, the salt pan is narrower when the potential evaporation rate is higher (e.g., Figure 4(e1)). Also, clearly, the width of salt pan also greatly depends on the slope of marsh platform. When the marsh surface becomes steeper while the other factors (e.g., potential evaporation rate, tidal amplitude) remain unchanged, the salt pan will be much narrower (e.g., Figure 4(e1) vs Figure 4(e2)). From Figures 4(e1)-4(e3), it can be inferred that large areas of salt

pans are more likely to be found in micro-tidal marshes that are mildly sloping and located at temperate climate zones.

4. Concluding Remarks

This study investigated the characteristics of salt pans in coastal marshes based on a 2-D creek-perpendicular cross section. Major findings from this study are:

(1) Under the continuous effect of evaporation, salinity near the marsh surface of the supratidal zone keeps rising, eventually leading to salt precipitation and the subsequent formation of a salt pan. Meanwhile, the accumulated salt in the marsh sediments create an upward salinity gradient that triggers unstable flow.

(2) The overall salt mass and the width of salinity plateau tend to decrease with the decline of potential evaporation rate, and the increase of either tidal amplitude or marsh platform slope.

(3) Consistent with the conclusions of previous studies, the locations of salt pans are within the salinity plateaus. Overall, the thickness of precipitated salt on the marsh surface will decrease when the potential evaporation rate declines, the tidal amplitude increases, or the marsh surface becomes steeper. Moreover, the salt pan is wider when the potential evaporation rate is lower, the tidal amplitude is smaller, and the marsh surface is mildly sloping.

Despite the above findings, this study used a simple semi-diurnal solar tidal signal, whereas the multi-constitute tides (e.g., spring-neap tides) may complicate the salt dynamics in coastal marshes. Moreover, our study considered a 2-D normal-creek section and neglected the 3-D topography, which has been found to significantly affect the porewater flow and salinity distribution patterns (Moffett et al., 2010b; Xin et al., 2011). In addition, the present study set a constant potential evaporation rate in each case, while in reality it may vary remarkably even during a day. These factors should be examined in future research to better characterize salt pans in coastal marshes. Despite these limitations, this study still provides a deep insight into the

features of hypersaline zones in salt marshes, thereby promoting a better understanding of the eco-functions of these wetlands. A systematic and quantitative examination of the salt pan characteristics in coastal marshes would not only advance our understanding of the marsh ecosystems but also provide guidance for developing effective measures to prevent them from degradation, causing unexpected release of blue carbon.

Acknowledgements

This study was financially supported by the Natural Science Foundation of China (41807178, 41976162, 51879088), the Natural Science Foundation of Jiangsu Province (BK20190023), and the Australian Research Council Discovery Project (DP180104156, DP19010372). The source code and model input are available at https://doi.org/10.6084/m9.figshare.19188464.v1.

References

Adam, P. (1990). *Saltmarsh Ecology*. Cambridge University Press.

America, I., Zhang, C., Werner, A. D., & van der Zee, S. E. A. T. M. (2020). Evaporation and Salt Accumulation Effects on Riparian Freshwater Lenses. *Water Resources Research*, *56*(12), e2019WR026380. https://doi.org/10.1029/2019WR026380

Bertness, M. D., & Pennings, S. C. (2000). Spatial variation in process and pattern in salt marsh plant communities in eastern north america. In M. P. Weinstein & D. A. Kreeger (Eds.), *Concepts and Controversies in Tidal Marsh Ecology* (pp. 39-57). Springer Netherlands. https://doi.org/10.1007/0-306-47534-0_4

Chapman, V. J. (1974). *Salt marshes and salt deserts of the world*. Cramer. https://books.google.com.au/books?id=dKUKAQAAIAAJ

Emery, N. C., Ewanchuk, P. J., & Bertness, M. D. (2001). Competition and salt-marsh plant zonation: Stress tolerators may be dominant competitors. *Ecology*, *82*(9), 2471-2485. https://doi.org/10.1890/0012-9658(2001)082[2471:CASMPZ]2.0.CO;2

He, Q., Cui, B., & An, Y. (2012). Physical stress, not biotic interactions, preclude an invasive grass from establishing in forb-dominated salt marshes. *PLoS ONE*, *7*(3), e33164. https://doi.org/10.1371/journal.pone.0033164

Hsieh, Y. P. (2004). Dynamics of tidal salt barren formation and the record of present-day sea level change. In *The Ecogeomorphology of Tidal Marshes* (pp. 231-245). American Geophysical Union. https://doi.org/10.1029/CE059p0231

Hughes, J. D., & Sanford, W. E. (2004). *SUTRA-MS, a version of SUTRA modified to simulate heat and multiple-solute transport* (Open-File Report 2004-1207, Issue. https://water.usgs.gov/nrp/gwsoftware/SutraMS/OFR2004-1207.pdf

Kirwan, M. L., & Megonigal, J. P. (2013). Tidal wetland stability in the face of human impacts and sea-level rise. *Nature*, *504*, 53. https://doi.org/10.1038/nature12856

Ledous, J., Alexander, C., & Meile, C. (2013). Delineating the drivers of groundwater flow at a back barrier island–marsh transect in coastal Georgia. 2013 Georgia

Water Resources Conference,

Mahall, B. E., & Park, R. B. (1976). The ecotone between Spartina Foliosa Trin and Salicornia Virginica L in salt marshes of Northern San Francisco Bay: II. Soil water and salinity. *Journal of Ecology*, *64*(3), 793-809. https://doi.org/10.2307/2258809

Moffett, K. B., Robinson, D. A., & Gorelick, S. M. (2010a). Relationship of salt marsh vegetation zonation to spatial patterns in soil moisture, salinity, and topography. *Ecosystems*, *13*(8), 1287-1302. https://doi.org/10.1007/s10021-010-9385-7

Moffett, K. B., Wolf, A., Berry, J. A., & Gorelick, S. M. (2010b). Salt marsh–atmosphere exchange of energy, water vapor, and carbon dioxide: Effects of tidal flooding and biophysical controls. *Water Resources Research*, *46*(10), W10525. https://doi.org/10.1029/2009WR009041

Noe, G. B. (2002). Temporal variability matters: Effects of constant vs. Varying moisture and salinity on germination. *Ecological Monographs*, *72*(3), 427-443. https://doi.org/10.1890/0012-9615(2002)072[0427:tvmeoc]2.0.co;2

Noe, G. B., & Zedler, J. B. (2000). Differential effects of four abiotic factors on the germination of salt marsh annuals. *American Journal of Botany*, *87*(11), 1679-1692. https://doi.org/10.2307/2656745

Pennings, S. C., Grant, M.-B., & Bertness, M. D. (2005). Plant zonation in low-latitude salt marshes: disentangling the roles of flooding, salinity and competition. *Journal of Ecology*, *93*(1), 159-167. https://doi.org/10.1111/j.1365-2745.2004.00959.x

Pennings, S. C., & Moore, D. J. (2001). Zonation of shrubs in western Atlantic salt marshes. *Oecologia*, *126*(4), 587-594. https://doi.org/10.1007/s004420000548

Shen, C., Jin, G., Xin, P., Kong, J., & Li, L. (2015). Effects of salinity variations on pore water flow in salt marshes. *Water Resources Research*, *51*(6), 4301-4319. https://doi.org/10.1002/2015WR016911

Shen, C., Zhang, C., Xin, P., Kong, J., & Li, L. (2018). Salt dynamics in coastal marshes: Formation of hypersaline zones. *Water Resources Research*, *54*(5),

3259-3276. https://doi.org/10.1029/2017wr022021

Voss, C. I., & Provost, A. M. (2008). *SUTRA: A model for saturated-unsaturated, variable-density groundwater flow with solute or energy transport* (Water Resources Investigation Report 02-4231, Issue. https://water.usgs.gov/nrp/gwsoftware/sutra/SUTRA_2_2-documentation.pdf

Wang, H., Hsieh, Y. P., Harwell, M. A., & Huang, W. (2007). Modeling soil salinity distribution along topographic gradients in tidal salt marshes in Atlantic and Gulf coastal regions. *Ecological Modelling*, *201*(3–4), 429-439. https://doi.org/10.1016/j.ecolmodel.2006.10.013

Wilson, A. M., & Gardner, L. R. (2006). Tidally driven groundwater flow and solute exchange in a marsh: Numerical simulations. *Water Resources Research*, *42*(1), W01405. https://doi.org/10.1029/2005WR004302

Xin, P., Yuan, L.-R., Li, L., & Barry, D. A. (2011). Tidally driven multiscale pore water flow in a creek-marsh system. *Water Resources Research*, *47*(7), W07534. https://doi.org/10.1029/2010WR010110

Xin, P., Zhou, T., Lu, C., Shen, C., Zhang, C., D'Alpaos, A., & Li, L. (2017). Combined effects of tides, evaporation and rainfall on the soil conditions in an intertidal creek-marsh system. *Advances in Water Resources*, *103*, 1-15. https://doi.org/10.1016/j.advwatres.2017.02.014

Zhang, C., Li, L., & Lockington, D. (2014). Numerical study of evaporation-induced salt accumulation and precipitation in bare saline soils: Mechanism and feedback. *Water Resources Research*, *50*(10), 8084-8106. https://doi.org/10.1002/2013WR015127

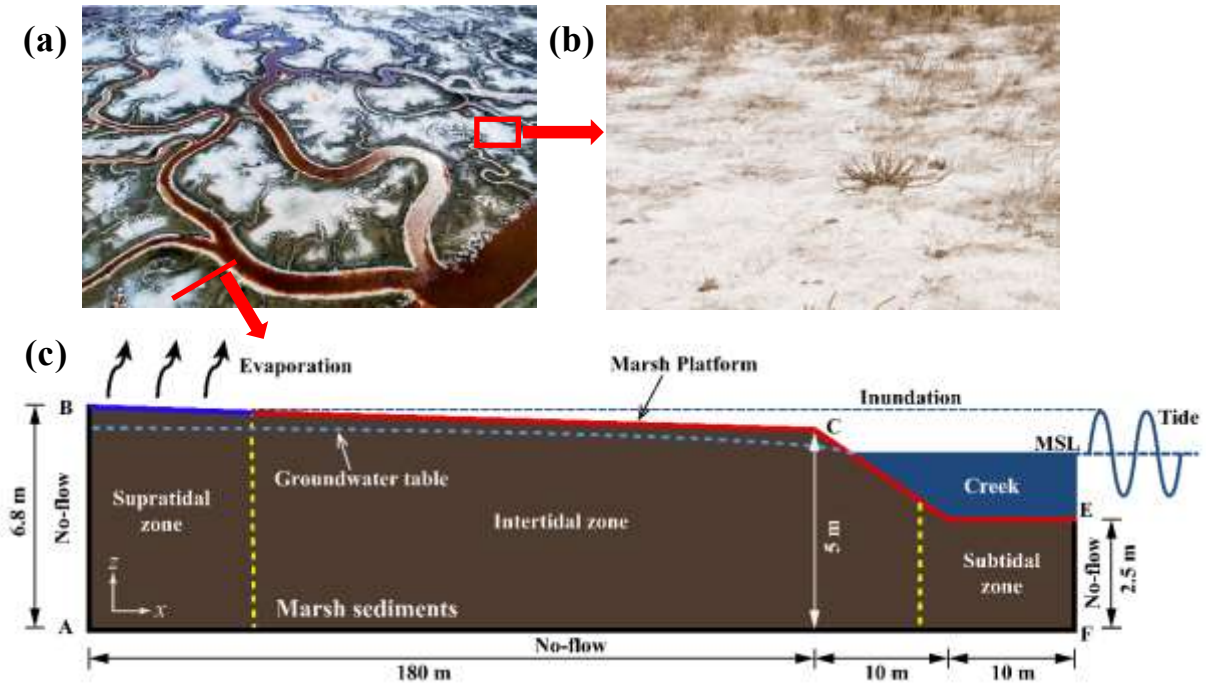

Figure 1. (a) Aerial view of a salt marsh with meandering tidal creeks and white salt pans at Alvisio. The photo was purchased at Masterfile: https://www.masterfile.com/image/en/6118-08827531/aerial-view-of-the; (b) A close look of salt pan in the supratidal zone of a salt marsh; (c) Schematic diagram of the 2-D numerical model domain representing a creek-perpendicular section of salt marshes and corresponding boundary conditions. Note that the inland boundary height of 6.8 m corresponds to a mash platform slope of 0.01, and may vary according to the slope used in different simulation cases.

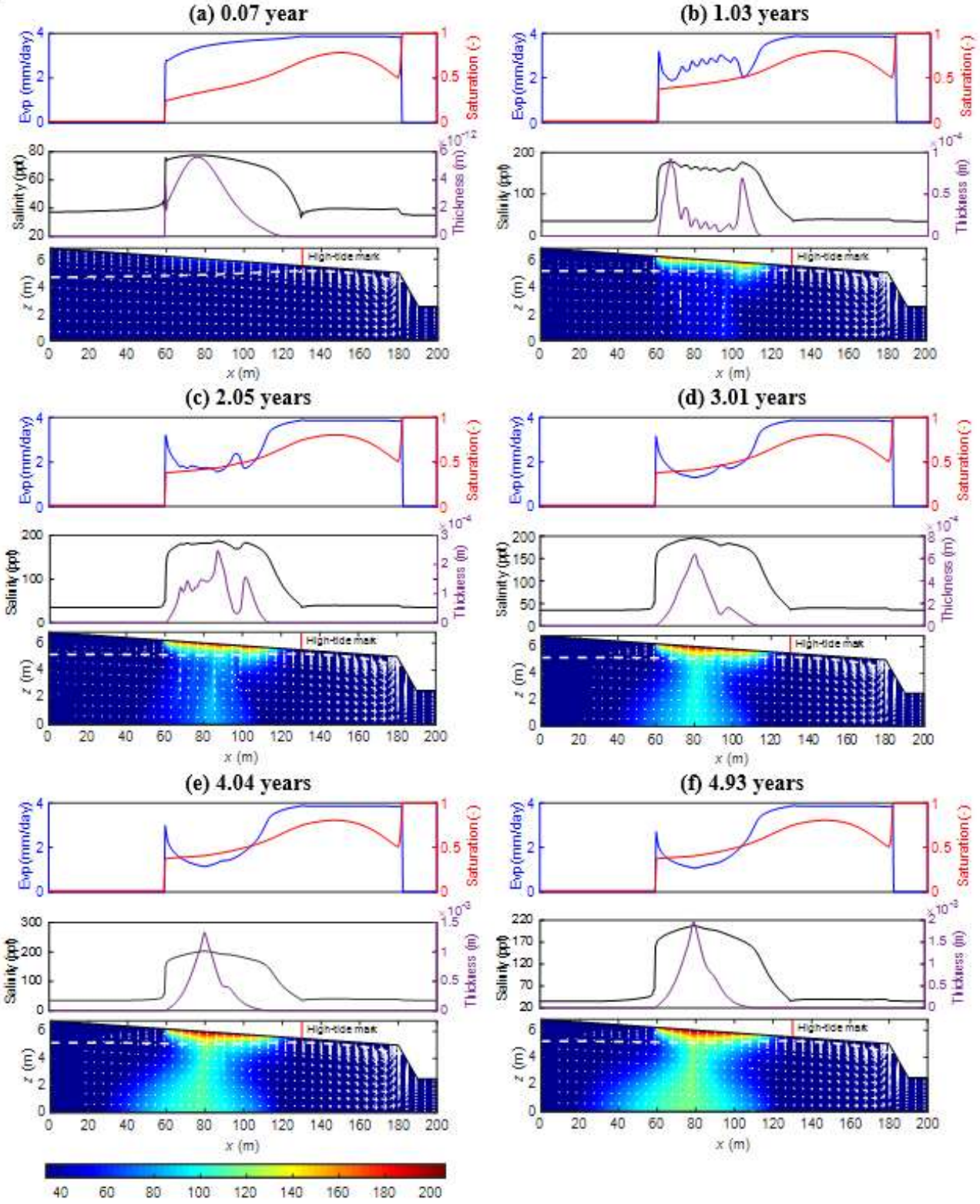

Figure 2. Time-dependent variations of evaporation rate, surface soil saturation, surface salinity, precipitated salt thickness, and salinity distributions for the case with marsh platform slope, potential evaporation rate and tidal amplitude being 0.01, 4 mm day^{-1} and 1.0 m, respectively. All the plots show conditions at mid rising tide. The white dashed line represents the water table, the white arrows indicate the groundwater flow field, and the red line represents the high-tide mark that separates the supratidal (left) and intertidal (right) zones.

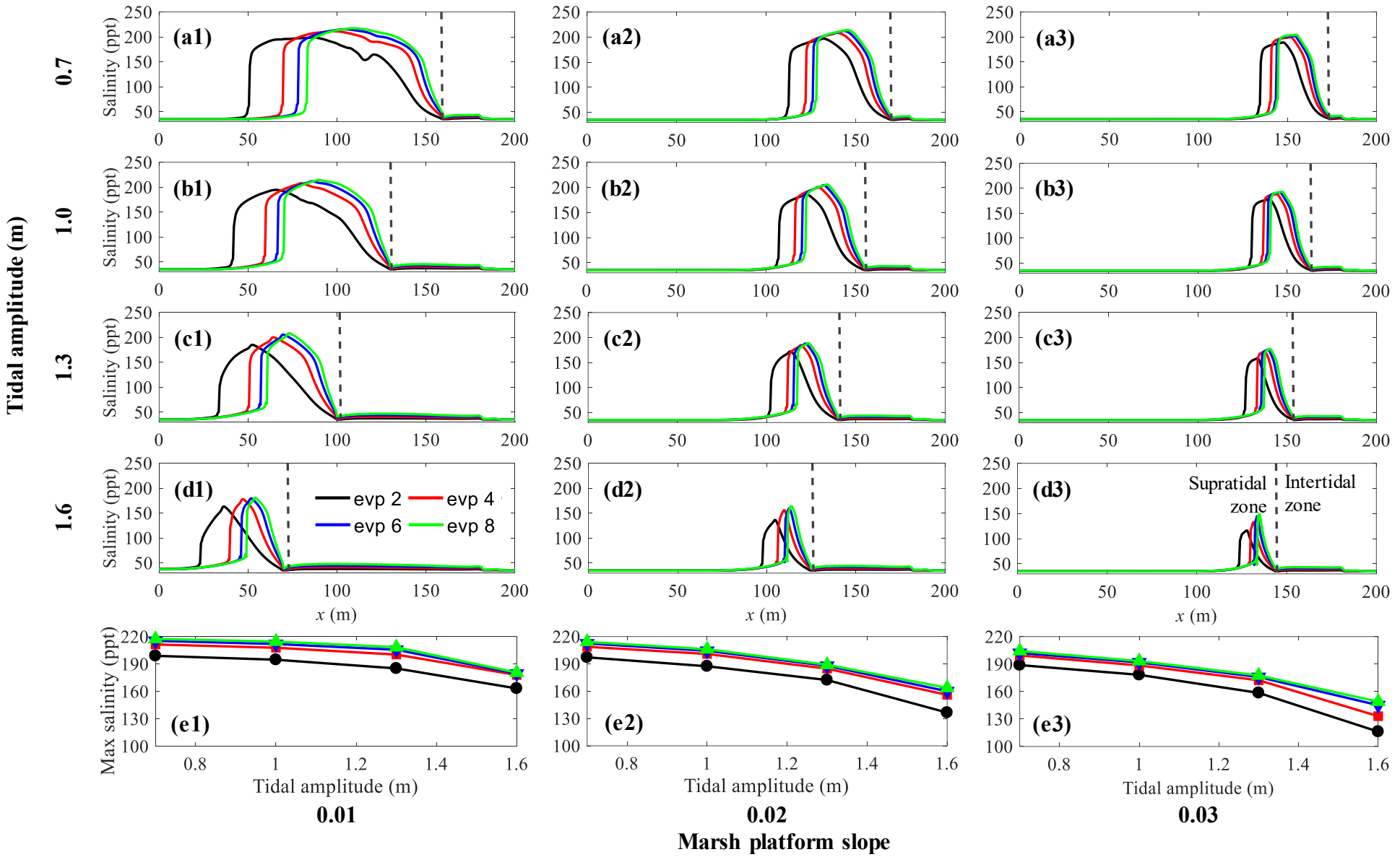

438 **Figure 3.** Comparison of (a1-d3) surface salinity distributions and (e1-e3) maximum surface salinity under different combinations of tidal amplitude, marsh

platform slope, and potential evaporation rate. The vertical dashed line represents the high tidal mark that separates supratidal and intertidal zones.

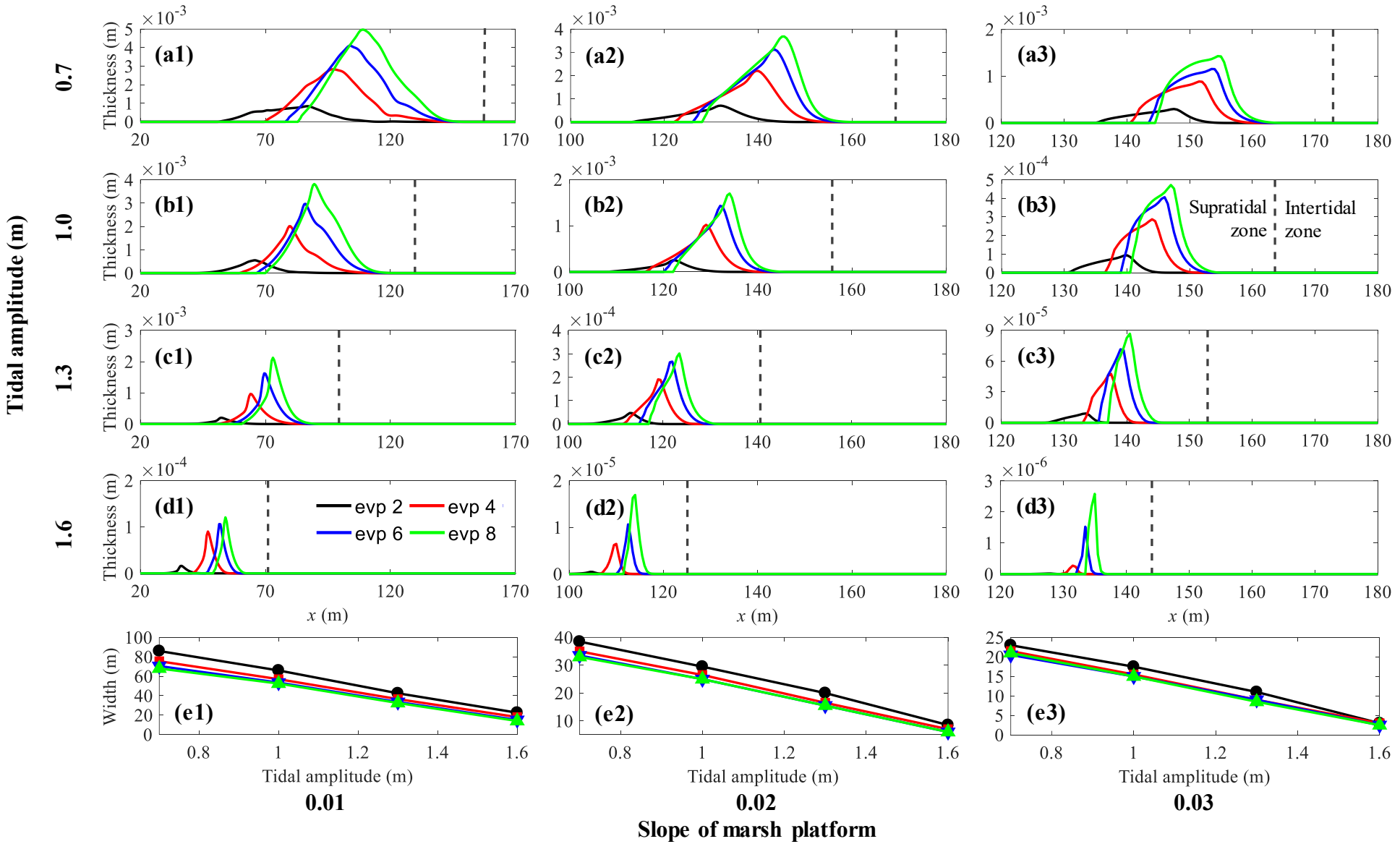

440 **Figure 4.** Comparison of (a1-d3) thickness of precipitated salt and (e1-e3) salt pan width under different combinations of tidal amplitude, marsh platform

slope, and potential evaporation rate. The vertical dashed line represents the high tidal mark that separates supratidal and intertidal zones.